Front. Electr. Electron. Eng. China 2007, 2(1): 83–87
DOI 10.1007/s11460-007-0015-x

RESEARCH ARTICLE

LI Chaobo, JIAO Binbin, SHI Shali, YE Tianchun, CHEN Dapeng, ZHANG Qingchuan, GUO Zheying, DONG Fengliang, WU Xiaoping

A novel MEMS-based focal plane array for infrared imaging

Abstract On the basis of opto-mechanical effect and micro electromechanical system (MEMS) technology, a novel substrate-free focal plane array (FPA) with the thermal isolated structure for uncooled infrared imaging is developed, even as alternate evaporated Au on SiN cantilever is used for thermal isolation. A human thermal image is obtained successfully by using the infrared imaging system composed of the FPA and optical detecting system. The experiment results show that the realization of thermal isolation structure in substrate-free FPA increases the temperature rise of the deflecting leg effectively, whereas the noise equivalent temperature difference (NETD) is about 200 mK.

Keywords MEMS, focal plane array (FPA), opto-mechanical, low-pressure chemical vapor deposition (LPCVD), SiN_x, NETD

1 Introduction

In recent years, a novel uncooled infrared imaging technology has been developed on the basis of micro electromechanical system (MEMS) fabrication technology and opto-mechanical effect [1–4]. Compared with the traditional cooled and uncooled detector, it will lead to wide applications with low cost, with no requirement of the costly cooler, and the complex readout circuit. Furthermore, the utmost detecting sensitivity by theoretical calculation can reach the order of μK [5]. This means this type of detector maybe have broad applications in the field of high performance infrared radiation (IR) detecting.

Opto-mechanical uncooled infrared imaging system consists of three components: IR lens, focal plane array (FPA), and optical readout, whereas optical readout is composed of optical-readable light, lens array, and optical filter. However, the heart of the system is the FPA, which is an array of many imaging pixels, and the pixel is made up of micro-mirror and bending organ with a generally used bimaterial structure. When the incident IR flux is absorbed by the pixel, the bimaterial legs will deflect for the temperature rise of the pixel and the mismatch of thermal expansion coefficient between the two materials. The temperature rise of each pixel is different, so it's deflecting angle or displacement is different too. Our goal is to detect these deflecting angles or displacements by optical readout and turn them into the corresponding thermal image.

Most of the earlier researches of the FPA are focused on sacrificial layer structure [1–4]. The basic idea is that there is a distance of about 2–3 μm between the substrate and the micro-cantilever and to fix each pixel on the substrate separately. The advantage of this structure is that the pixels are nested in each other and the device has a high-duty factor. But for the survival of the silicon substrate, the shortcoming is that the reflecting and absorbing by the substrate cause over 40% of the incident IR energy unable to reach the detecting arrays; on the other hand, the releasing process of the complex sacrificial layer easily leads to conglutination between the two parts to invalidate the suspended structure [6]. As reported in the earlier works [1–4], the best value of the noise equivalent temperature difference (NETD) is about 1 K.

To eliminate such problems, a novel substrate-free FPA was developed in this group in 2004 and the corresponding IR images of the target object at 200 mK °C was obtained and the NETD was about 7 K [7]. The basic idea of this structure is that there is no silicon substrate under the active parts. The advantages of this structure are: 1) no IR reflection by the substrate and high IR absorbility; 2) no need of sacrificial layer– releasing process, easy to fabricate and low blind-pixel ratio. However, the bending legs are not long enough to make the temperature resolution low for the reason that there

Translated from *Chinese Journal of Semiconductors*, 2006, 27(1): 150–155 [译自: 半导体学报]

LI Chaobo, JIAO Binbin, SHI Shali, YE Tianchun,
CHEN Dapeng (✉)
Micro-Processing and Nano-Technology Department, Institute of Microelectronics, Chinese Academy of Sciences, Beijing 100029, China
E-mail: chendp@sohu.com

ZHANG Qingchuan, GUO Zheying, DONG Fengliang, WU Xiaoping
Key Laboratory of Mechanical Behavior and Design of Materials, University of Science and Technology of China, Hefei 230027, China

is no thermal isolation structure. To improve the bending performance and the temperature resolution, a novel substrate-free detector with multi-fold legs and an interval gild structure was designed and fabricated. With the optical readout system, the IR image of the human body was obtained successfully at the room temperature. The NETD was about 200 mK.

2 Material selections for FPA

Generally the pixel consists of three components: micro-mirror for IR absorbing and reflecting visible light, bimaterial cantilever for bending, and single-material cantilever for thermal isolation. According to the device structure and the fabrication process, the two materials selected had to meet the following basic requirements First, one of the two materials should be good IR absorber. Second, one of the two materials should have good ability to reflect readout visible light. Third, the difference of the thermal expansion coefficients between the two materials is as large as possible. That means the bending of the bimaterial cantilever should be as big as possible with the same temperature rise. Fourth, one of the two materials should have low thermal conductive coefficient to be a single material cantilever for thermal isolation. Fifth, both of the two materials should have low remnants stress. Sixth, the two materials should not be removed by KOH in the step of wet etch Si.

Table 1 [2] shows the generally used bimaterial combination. SiN_x and SiO_2 are used as IR absorbing materials, whereas Au and Al are used as reflectors to reflect visible light. For the reason that Al and SiO_2 cannot survive in our wet etching step, low-pressure chemical vapor deposition (LPCVD) low stress SiN and Au were selected as the two materials for constructing the bimaterial cantilever. From Table 1, it is seen that SiN_x and Au can form bimaterial bending cantilever for they have large mismatch of thermal expansion coefficients, whereas SiN_x can be the single material cantilever for thermal isolation because of its very small thermal conductive coefficient.

Table 1 Mechanical and thermal properties of several materials used usually

	Young's modules /GPa	Thermal conductive coefficient /($W \cdot m^{-1} \cdot k^{-1}$)	Thermal expansion coefficient /($10^{-6} \cdot K^{-1}$)	Heat capacity /($J \cdot kg^{-1} \cdot K^{-1}$)	Intensity /($10^3 Kg \cdot m^{-3}$)
SiN_x	180	5.5 ± 0.5	0.8	691	2.40
Au	73	296.0	14.2	129	19.30
SiO_2	46–92	1.1	0.05–12.3	–	2.20
Al	80	237.0	23.6	908	2.70

Figure 1 [2] shows the refractive index of LPCVD SiN_x in the band of infrared radiation. The imaginary part indicates the IR absorbing characteristic of SiN_x. It can be seen that

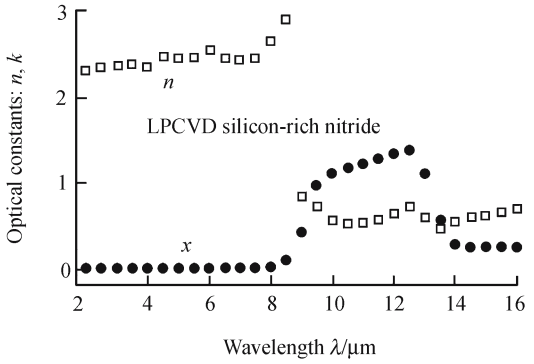

Fig. 1 Real (n) and imaginary (k) parts if of the refractive index of LPCVD SiN_x

SiN_x has high absorptivity to infrared radiation with the band 8–14 μm (the corresponding band of human body's radiation).

3 Low stress SiN_x film

SiN_x film has broad uses in MEMS area, but its tensile stress after the general preparation process and the stress that develop rapidly with the increase in film thickness. However, the substrate-free structure that was designed required that the film should be tough enough and have relatively large amount of the thickness (0.5–2 μm) and area (20 mm × 20 mm). The LPCVD process was selected to develop low stress SiN_x film.

The process started with P〈100〉 double-side polished silicon wafer. Before deposition, the wafer was treated with the general cleaning process, and then was put into the quartz tube to be deposited with double-side SiN_x. The reactant gases are SiH_2Cl_2 and NH_3. Such parameters as the flow rate of the reactant gases, the pressure in the tube and the deposition temperature can be all controlled, and by adjusting the above parameters, many SiN_x films can be obtained with different internal structure. After deposition, the substrate-free SiN_x film was fabricated by dry etching the SiN_x deposited on the backside of the Si wafer to form the etch window and subsequently to etch the silicon wafer through the window in KOH solution.

From the experiment, the following results were found. To form substrate-free structure, tensile stress is necessary in SiN_x film, and the appropriate quantity of stress should be controlled in the range of 10^7–10^8 Pa (Fig. 2). If the tensile stress is too big, the film will break up, and the compressive stress will result in the film curling. When analyzing the transmission electron microscope (TEM) photographs of the films that can form the substrate-free structure well, it can be seen that the silicon-embedded structure in all the films are similar to what Fig. 2 shows. But in the TEM photograph of the breaking and curly films, such silicon-embedded structure cannot be seen. These SiN_x films have been proved to be low-stress embedded combination film with a large number of partly crystal silicon microstructure with uniform distribution and of moderate dimension [8].

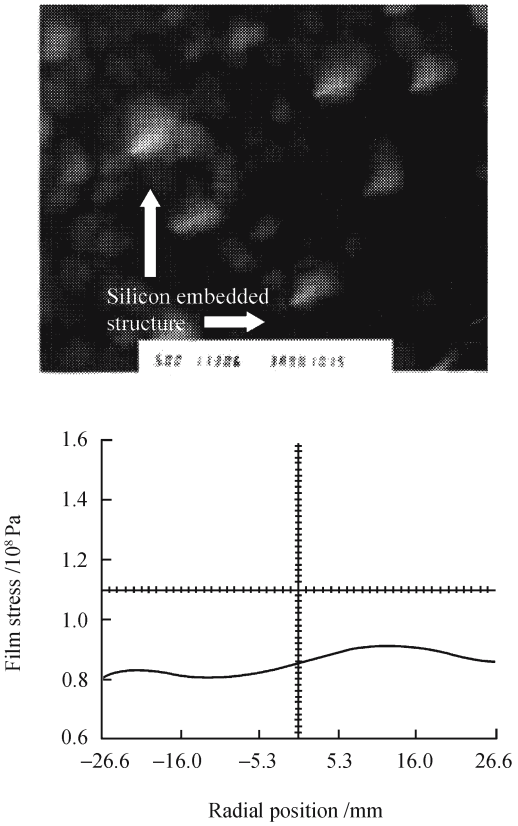

Fig. 2 TEM micrograph and planar stress distribution graph of substrate-free SiN_x film

4 FPA structure

The substrate-free FPA that was designed is an array with 100×100 pixels. All the FPA consisted of the pixels and the supporting frame. Meanwhile, one single pixel has the area of 200 μm × 200 μm, and all the substrate-free area is 20 mm × 20 mm. Each pixel was composed of an IR absorbing board and two bending sections that were symmetrically located at both sides of the IR absorbing board and fixed on the supporting frame. The IR absorbing board was SiN_x/Au bimaterial structure, whereas SiN_x was used to absorb infrared radiation and Au was used to reflect readout visible light. The bending section was composed of the bending cantilevers and the thermal isolation cantilevers with two folds and alternate distribution, whereas bending cantilever was SiN_x/Au bimaterial structure and the thermal isolation cantilever was single material structure. To replace the bending structure with entire gilt on all the legs with that of folds and alternation can increase the total length of the bending legs effectively. Its function is like the effect of the superposition of the bending of all the legs [6]. The main fabrication process is shown in Fig. 3. Figure 4 shows the scanning electron microscope (SEM) photograph of a part of the FPA that was prepared, and the top-right inserted photograph shows the structure of one pixel clearly.

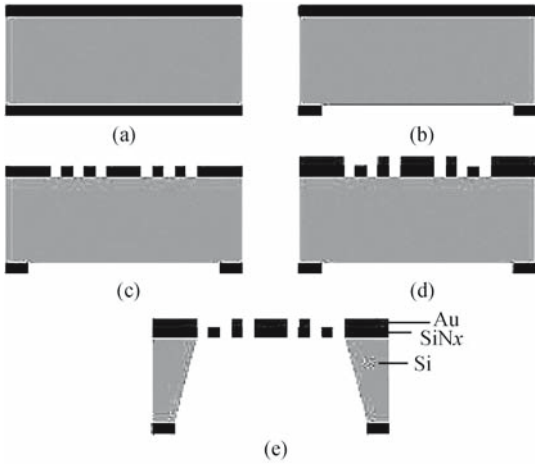

Fig. 3 Main steps of the fabrication process of FPA

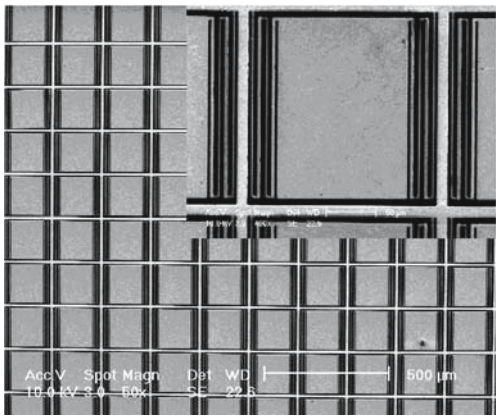

Fig. 4 Electron micrograph of a part of the FPA, the top-right inserted photo shows the structure of one pixel clearly

5 Imaging experiment, result, and discussion

5.1 Optical readout design

The optical readout that was employed is the incoherent light readout method. The working principle is shown in Fig. 5. The parallel light arrived at the FPA and was reflected, and the reflected light passed through lens 1 that serves as transforming lens. Then the zero-order spectra of the FPA were synthesized by the knife-edge filter placed on the focal plane of lens 2 that works as an imaging lens. Consequently, by using the charge coupled device (CCD) camera, the deflecting angle of the cantilever was detected and was converted to the gray level change in the CCD and imaged.

5.2 Imaging experiment

To combine the FPA, the above optical readout system was prepared, and the imaging experiment was done. IR lens with f number of 0.7 was employed. Meanwhile, the FPA was

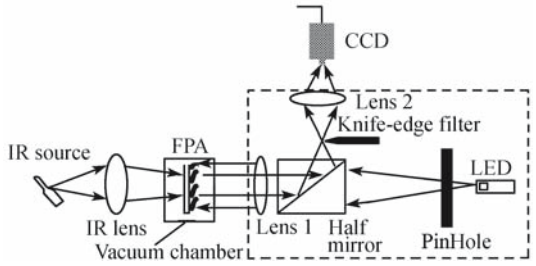

Fig. 5 Working principle of the optical readout system

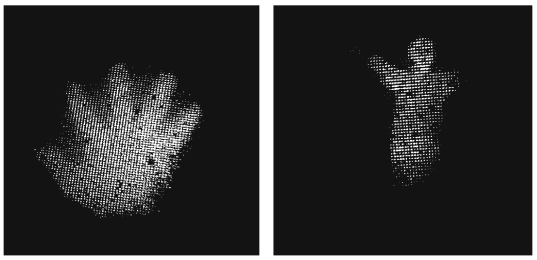

Fig. 6 IR images of a person and his hand

sealed into the vacuum chamber (~1 Pa) to decrease the effect of convection and flow of the air.

Figure 6 shows two IR images of a person and his hand. The person and his hand were located at 5 m and 1 m away from the IR lens at different times. It can be seen that the profile of the palm is relatively clear, but only a rough outline can be identified between every two closest fingers. That is because the heat disturbance between the close pixels leads to the presence of the same gray level between the close pixels. In the IR image of the person, the profile of the person can be distinguished clearly.

5.3 System detection sensitivity and noise level analysis

To evaluate the performance of the infrared imaging system NETD is an important parameter. It denotes the temperature difference when the corresponding output signal (the gray level N) of the area of the target object with the temperature difference ΔT_s is equal to detector's own noise signal (the gray level N_{noise}). It can be described as

$$\text{NETD} = \Delta T_s \frac{N_{\text{noise}}}{N} = \frac{N_{\text{noise}}}{N/\Delta T_s} \tag{1}$$

where $N/\Delta T_s$ is the system's thermal response sensitivity and is defined as the gray level change when unit temperature of the IR object changes. The noise and thermal response sensitivity of the system was detected by the following steps.

1) To detect the gray level N_{noise} of the system noise, 32 images of background were collected without target objects, then the histogram of the noise fluctuation as shown in Fig. 7 was calculated. Because most of the noise was distributed around the corresponding gray level of the maximum probability, this corresponding gray level can be considered

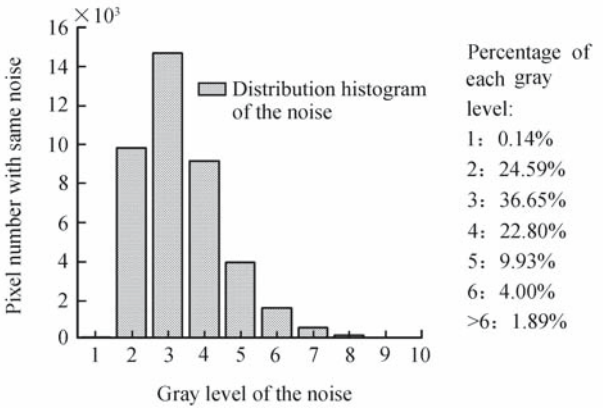

Fig. 7 Noise distribution of the system

as the system noise N_{noise}. The result of the calculation shows N_{noise} is 5.

2) To detect the system's thermal responsivity, the corresponding response of the temperature difference between the target object and the background was confirmed, and then the system's thermal responsivity was calculated. The background temperature was 27.47°C and was derived from the mean of the readings of three different thermometers (Table 2); the average temperature of the hand is about 35°C by using the commercial infrared camera; thus the average temperature difference between the hand and the background is about 7.53°C. Then six regions with 3×3 pixels were selected in different areas of the hand's thermal image, six pixels were chosen with relatively high gray level and their gray levels N were detected (Table 3). The statistical mean of the corresponding response of the hand is 194.

Table 2 The temperature of background measured by three thermometers

Thermometer type	Digital thermometer	Alcohol thermometer	Mercury thermometer
Background temperature /°C	27.9	27.5	27.0

Table 3 Gray level of the pixels for testing

Pixel number	1	2	3	4	5	6
Gray level	213	211	167	152	183	238

According to Eq. (1), when N and ΔT_s employed the average value respectively, the NETD is 0.194 K; when N employed 152, the minimum value, the NETD is 0.247 K; when N is 238, the maximum value, the NETD is 0.158 K.

From the above analysis, the average NETD of the system is about 200 mK, whereas the highest and the lowest NETD of a single pixel are 158 mK and 247 mK respectively. This results in an un-uniform fabrication of the array device. If optimization to the fabrication process is done more, the performance of the device will be better, including the controlling of the internal stress of the membranes, lithography, and etching steps.

5.4 Limitation and future works

From Fig. 6, it can be seen that the temperature distribution and the details of the human body are not clear enough, except for the parts with different temperature. This condition is mainly because the detective sensitivity and resolution are not good enough. To increase the performance of the FPA, several factors, such as the material selection, structure and fabrication design must be considered synthetically.

The two materials that were selected are low stress SiN_x and Au, which are not the optimized ones though they meet the requirements of small Young's modules and large difference of thermal expansion coefficients. From Fig. 1, it is seen that the Young's modules of SiO_2 are smaller than that of SiN_x and the difference in thermal expansion coefficients between SiO_2/Al, SiO_2/Au, and SiN_x /Al are all greater than that of SiN_x /Au. According to the principle of materials mechanics, the bending effect of the combination of SiO_2/Al, SiO_2/Au, and SiN_x /Al will be better than that of SiN_x /Au if the device structures are the same. But SiO_2 and Al were the functional materials because these two materials can be removed by KOH in the step of wet-etching Si substrate. With the development of new fabrication process, a combination these three new materials can be used to obtain higher detecting sensitivity.

To improve the resolution, the pixel area should be reduced, and a high enough detecting sensitivity should be maintained. According to the knowledge of the materials mechanics, when the deflection of Bi-material (BM) cantilever has reached equilibrium state, the deflection quantity can be expressed as

$$\delta = \frac{6(\alpha_2 - \alpha_1)\Delta T(n + \frac{1}{P})L^2}{h_1} \tag{2}$$

$$P = \frac{(n^2\phi - 1)^2 + 4n(n^2 + 2n + 1)\phi}{n\phi} \tag{3}$$

where δ is the displacement of the free end, α the thermal expansion coefficients, L length of the leg, h_1 the cantilever thickness, ΔT the temperature change, n the thickness ratio between the two materials, $\phi = E_2/E_1$ and E is the elastic modulus.

To analyze Eq. (2) and Eq. (3), for a predetermined thickness and with same temperature rise, the displacement is highest when the thickness ratio between two materials is equal to the inverse ratio of the square root between them, and the displacement is the inverse ratio of the total thickness.

When the total thickness of the cantilevers was being decreased, it increased the resolution while maintaining relatively high sensitivity to reduce the total length of the cantilever. As for the limitation of the fabrication technology, the structure that was designed to employ the combination of 2 μm SiN_x and 0.2 μm Au was far from the optimized one. By improving the shortcomings in the fabrication process, such as film deposition and the etching damage, the device array with a smaller pixel size can be achieved to improve the resolution.

6 Conclusions

A novel MEMS-based bimaterial substrate-free focal plane array with multi-fold legs and interval gild structure was designed and fabricated. Substrate-free structure can solve the problem of IR reflection by the substrate very well, and multi-fold and interval gild structure functions as the bending parts with the effect of the superposition of multi-level deformation of multi-level enhancement. LPCVD low stress SiN_x and Au were the two materials used to form the bimaterial structure. The fabrication process is relatively easier than the sacrificial layer technology. With the optical readout system, the IR image of the human body was obtained successfully. The average NETD was about 200 mK. If more optimization was done on materials selection, device structure, and fabrication process, a better result can be obtained.

Acknowledgements This work was supported by the National Natural Science Foundation of China (Grant No. 60236010), the National Technology Research Development Program of China (No. 2005AA404210).

References

1. Mao M, perazzo T, Kwon O, et al. Direct-view uncooled micro-optomechanical infrared camera. MEMS '99, Twelfth IEEE International Conference on, 17–21 Jan, 1999: 100–105
2. Zhao Y. Optomechanical uncooled infrared imaging system. Dissertation of UC, Berkeley, 2002
3. Ishizuya T, Suzuki J, Akagawa K, et al. 160 × 120 pixels optically readable biomaterial infrared detector. Proc. of IEEE MEMS, 2002: 578–581
4. Duan Zhihui, Zhang Qingchuan, Wu Xiaoping, et al. Uncooled optical readable biomaterial micro-cantilever infrared imaging device. Chinese Physics Letters, 2003, 20(12): 2130–2132
5. Lai J, Perazzo T, Shi Z, et al. Optimization and performance of high-resolution micro-optomechanical thermal sensors. Sensors and Actuators A, 1997, 58: 113–119
6. Pan Liang. Focus plane array and readout system based on MEMS and visible light. Dissertation of USTC, 2004 (in Chinese)
7. Pan Liang, Zhang Qingchuan, Wu Xiaoping, et al. MEMS based optomechanical infrared imaging. Experimental Mechanics, 2004, 19(4): 403–407 (in Chinese)
8. Chen Dapeng, Ye Tianchun, Xie Changqing, et al. Study of SiN*x* film stress inlaid with silicon nanocrystals preparing by LPCVD. Chinese Journal of Semiconductors, 2001, 22(12): 1529–1533 (in Chinese)